



Published in final edited form as:

Clin Cancer Res. 2020 November 15; 26(22): 6003–6016. doi:10.1158/1078-0432.CCR-20-1523.

PD1 blockade enhances ICAM1-directed CAR T therapeutic efficacy in advanced thyroid cancer

Katherine D. Gray^{#1}, Jaclyn E. McCloskey^{#2}, Yogindra Vedvyas^{#2}, Olivia Kalloo¹, Steve El Eshaky¹, Yanping Yang², Enda Shevlin², Marjan Zaman², Timothy Ullmann¹, Heng Liang¹, Dessislava Stefanova¹, Paul J. Christos³, Theresa Scognamiglio⁴, Andrew Tassler⁵, Rasa Zarnegar¹, Thomas J. Fahey III¹, Moonsoo M. Jin², Irene M. Min¹

¹Department of Surgery, Weill Cornell Medicine, 1300 York Avenue, New York, NY 10065;

²Department of Radiology, Weill Cornell Medicine, 1300 York Avenue, New York, NY 10065;

³Department of Population Health Sciences, Weill Cornell Medicine, 1300 York Avenue, New York, NY 10065;

⁴Department of Pathology, Weill Cornell Medicine, 1300 York Avenue, New York, NY 10065;

⁵Department of Head and Neck Surgery, Weill Cornell Medicine, 1300 York Avenue, New York, NY 10065

These authors contributed equally to this work.

Abstract

Purpose: Advanced thyroid cancers, including poorly differentiated and anaplastic thyroid cancer (ATC), are lethal malignancies with limited treatment options. The majority of ATC patients have responded poorly to programmed death 1 (PD1) blockade in early clinical trials. There is a need to explore new treatment options.

Experimental Design: We examined the expression of PD-L1 (a ligand of PD1) and intercellular adhesion molecule 1 (ICAM1) in thyroid tumors and ATC cell lines, and investigated

Corresponding Authors: Thomas J. Fahey III; Department of Surgery, Weill Cornell Medicine, 1300 York Avenue, New York, NY 10065. Phone: 212-746-5130. tjfahey@med.cornell.edu; Moonsoo M. Jin; Department of Radiology, Weill Cornell Medicine, 1300 York Avenue, New York, NY 10065. Phone: 508-397-4342. moj2005@med.cornell.edu; Irene M. Min; Department of Surgery, Weill Cornell Medicine, 1300 York Avenue, New York, NY 10065. Phone: 212-746-5187. irm2226@med.cornell.edu.

Author's contributions

Conception and design: I.M. Min, M.M. Jin, T.J. Fahey

Development of methodology: K.D. Gray, J. McCloskey, Y. Vedvyas, E. Shevlin, I.M. Min, M.M. Jin

Acquisition of data (provided animals, acquired and managed patients, provided facilities, etc.): K.D. Gray, J. McCloskey, Y. Vedvyas, O. Kalloo, S. El Eshaky, Y. Yang, E. Shevlin, T. Ullmann, H. Liang, D. Stefanova, M. Zaman, T. Scognamiglio, A. Tassler, R. Zarnegar, T. J. Fahey, I.M. Min, M.M. Jin

Analysis and interpretation of data (e.g., statistical analysis, biostatistics, and computational analysis): K.D. Gray, J. McCloskey, Y. Vedvyas, O. Kalloo, S. El Eshaky, E. Shevlin, M. Zaman, P. J. Christos, I.M. Min, M.M. Jin

Writing, review, and/or revision of the manuscript: K.D. Gray, J. McCloskey, M.M. Jin, T.J. Fahey, Y. Yang, D. Stefanova, P. J. Christos, E. Shevlin, I.M. Min

Administrative, technical, or material support (i.e., reporting or organizing data, constructing databases): K.D. Gray, J. McCloskey, I.M. Min

Study supervision: I.M. Min

Disclosure of Potential Conflicts of Interest: P.J. Christos reports grants from Weill Cornell Clinical and Translational Science Center during the conduct of the study. R. Zarnegar reports personal fees from Beckton Dickenson outside the submitted work. No potential conflicts of interest were disclosed by the other authors.

the PD1 expression level in peripheral T cells of thyroid cancer patients. Next, we studied the tumor targeting efficacy and T cell dynamics of mono- and combination treatments of ICAM1-targeting CAR T cells and anti-PD1 antibody in a xenograft model of ATC.

Results: Advanced thyroid cancers were associated with increased expression of both ICAM1 and PD-L1 in tumors, and elevated PD1 expression in CD8⁺ T cells of circulating blood. The expression of ICAM1 and PD-L1 in ATC lines was regulated by the IFN γ -JAK2 signaling pathway. ICAM1-targeted CAR T cells, produced from either healthy donor or patient T cells, in combination with PD1 blockade demonstrated an improved ability to eradicate ICAM1-expressing target tumor cells compared to CAR T treatment alone. PD1 blockade facilitated clearance of PD-L1 high tumor colonies and curtailed excessive CAR T expansion, resulting in rapid tumor clearance and prolonged survival in a mouse model.

Conclusions: Targeting two IFN γ -inducible, tumor-associated antigens - ICAM1 and PD-L1 - in a complementary manner might be an effective treatment strategy to control advanced thyroid cancers *in vivo*.

Keywords

chimeric antigen receptor; thyroid cancer; ICAM-1; intercellular adhesion molecule-1; immune checkpoint; PD1; PD-L1; anaplastic thyroid cancer; adoptive T cell therapy; CAR-T cell therapy; xenograft

INTRODUCTION

Thyroid cancer is a common malignancy with increasing incidence (1). As tumors acquire increasing mutational burden, they undergo progression from well-differentiated papillary thyroid cancer (WDPTC) to poorly differentiated thyroid cancer (PDTC) and finally anaplastic thyroid cancer (ATC) (2). Patients with PDTC and ATC have disease-specific mortality rates that range between 40 – 100%, and these radioiodine-refractory tumors generally have a poor response to known systemic therapies (3,4). Monotherapies for PDTC/ATC targeting specific oncogenic molecules, such as BRAF and other kinase inhibitors, have also shown limited response in clinical trials (5,6). Recently, the FDA approved the combination treatment with inhibitors of BRAF and MEK for metastatic BRAF-mutant ATC (7). However, since the BRAF mutation (V600E) occurs in less than 30% of ATCs (2,8), the majority of ATC patients will not benefit from this combination therapy.

Recently, blockades of the immunosuppressive interaction between programmed cell death protein 1 (PD1) and its ligand (PD-L1) have generated considerable interest within the solid tumor field due to durable response rates observed in melanoma and lung cancer (9–13). Monoclonal antibodies that target PD1 expressed by T cells improve the function of exhausted T cells by blocking PD1 binding to PD-L1 that is expressed in the tumor. Histopathologic reports show that PD-L1 and PD1 proteins are upregulated in PDTC and ATC tumors and tumor infiltrating lymphocytes, respectively, suggesting a potential opportunity for immune checkpoint therapy in advanced thyroid tumors (14–16). However, the initial reports of pembrolizumab (anti-PD1) monotherapy to treat advanced thyroid

cancer have been disappointing, resulted in a response rate of less than 10% of the phase I clinical trials (17). Another clinical study using the anti-PD1 antibody, spartalizumab, reported a 17% overall response rate in ATC patients (18). Therefore, there is still a clear need to broaden treatment options.

Previously, our group demonstrated that intercellular adhesion molecule 1 (ICAM1, CD54), a cell surface glycoprotein with cytokine-inducible expression and known roles related to T lymphocyte trafficking in the endothelium (19), displays high levels of membranous expression in aggressive PTC, PDTC, and ATC malignant cells (20,21). We have also shown that human T cells transduced with a lentiviral vector encoding a third-generation chimeric antigen receptor (CAR) construct targeting ICAM1 (either via a single-chain fragment variable (scFv) derived from the R6.5 monoclonal antibody or an affinity-tuned natural ligand inserted (I) domain derived from integrin called lymphocyte function-associated antigen (LFA)-1)) selectively eradicated ATC cells in an ICAM1-dependent fashion in a preclinical murine model (21,22). Furthermore, these ICAM1-targeting CAR T (ICAM1-CAR T) cells can be tracked *in vivo* either optically by incorporation of *Renilla* luciferase or via PET/CT by incorporation of a radioligand-sensitive receptor, somatostatin receptor 2 (SSTR2), to examine kinetics of T cell distribution in response to tumor recognition (23).

Despite promising initial results of CAR T therapy in a number of solid tumors, its efficacy in general has been limited against solid tumors when compared to hematologic malignancies in part due to the highly immunosuppressive tumor microenvironment of solid tumors (24–28). Multiple specific tumor escape mechanisms have been proposed (29,30), including upregulation of PD1 expression on tumor-infiltrating CAR T cells. PD1 belongs to the immunoglobulin superfamily, and its expression on T cells is upregulated upon interaction with ligands PD-L1 and PD-L2 (12). The engagement of PD1 with PD-L1 inhibits T cell-mediated effector functions, conferring tumor protection against immune-mediated destruction (25).

In this study, we addressed the potential of an anti-PD1 antibody to rescue exhausted ICAM1-CAR T cells in a mouse model of ATC. Noting the upregulation of PD-L1 in thyroid tumors with aggressive histopathological features (14,16), we aimed to enhance the efficacy of ICAM1-CAR T cells via co-treatment with anti-PD1 monoclonal antibody. We first demonstrated increased membranous expression of ICAM1 and PD-L1 in PDTC and ATC tumors, and increased PD1 expression in CD8⁺ T cells from the patients' peripheral blood. Next, we showed that PD1 blockade boosted CAR T cells' ability to eradicate ICAM1-expressing target cells, caused by an increased propensity for CAR T cells to localize and eliminate tumor cells at a faster rate. PET/CT imaging of CAR T cells also revealed that PD1 combination led to lower expansion of CAR T cells than CAR T treatment alone. Our findings indicate that PD1 blockade plays a crucial role in reversing the immune checkpoint pathways upregulated in CAR T cells when CAR T cells are engaged in target tumor lysis and IFN γ -Jak2-signaling pathway activation, and may limit systemic toxicity that are frequently observed in CAR T therapy in patients.

MATERIALS AND METHODS

Sample collection and regulatory approval

Studies were conducted in accordance with the Declaration of Helsinki. Informed written consents were obtained from patients with a diagnosis of WDPTC, PDTC, or ATC pre-operatively for study enrollment between the years 2004–2019 under Weill Cornell Medicine Institutional Regulatory Board approval. Archived paraffin-embedded tissue blocks were retrieved from all patients with PDTC or ATC and a random sampling of PTC controls for immunohistochemistry (n=33). A subset of patients (n=15) was available for peripheral blood analysis either at the time of diagnosis or recurrence, and these samples were included for subsequent analysis as described. 10–20 cc of peripheral blood was collected from each patient in EDTA-containing tubes. Clinical characteristics of the patients and tumors were collected via chart review.

Peripheral blood samples and lymphocyte expansion

Fresh peripheral blood mononuclear cells (PBMCs) were extracted in Ficoll-Paque PLUS (GE Healthcare) density media using SepMate™ Isolation Tubes (STEMCELL Technologies). PBMCs were cultured overnight at a density of $>10^6$ cells/mL in OpTmizer CTS T-cell Expansion media (ThermoFisher) with 5% human AB serum (Sigma-Aldrich). Nonadherent PBMCs were collected and either used for flow cytometric analysis or enriched for T cells by using Dynabeads Human T-Cell Expander CD3/CD28 (ThermoFisher) at a 2:1 bead:T cell ratio in combination with OpTmizer media supplemented with recombinant human 12.5 ng/ml IL7 and 12.5 ng/ml IL15 (all cytokines from Peprotech). These T cells were expanded and maintained at constant density until lentiviral transduction of the ICAM1-CAR construct. For *in vivo* studies, a frozen leukopak was used for donor T cells which were cultured using the CliniMACS Prodigy (Miltenyi biotec) according to a protocol previously reported (31).

Culture of cell lines

The 8505C BRAF-mutated ATC cell line was obtained from DSMZ; HeLa cervical cancer cells and HEK 293T human embryonic kidney cells were obtained from ATCC. The JV cell line was derived previously by our group from fresh tissue culture of a surgical ATC tumor specimen and was used to establish patient-derived xenograft model (21). FRO and KHM-5M cell lines were generously provided by Dr. Juillard's laboratory at UCLA and Dr. Fagin's laboratory at MSKCC, respectively. All epithelial cell lines were cultured in RPMI media supplemented with 10% fetal bovine serum (FBS) at 37°C with 5% CO₂. Cell lines were stably transduced with a lentiviral vector encoding fLuc-F2A-GFP lentivirus (Biosettia) and were used in effector to target (E:T) experiments and *in vivo* tracking within xenograft models. Mycoplasma detection assay (Lonza) was routinely conducted to rule out contaminated cell lines.

Flow cytometry

Anti-human ICAM1-APC/Fire 750 (clone HA58, BioLegend) and anti-human PD-L1-APC (clone 29E.2A3, BioLegend) were used to characterize protein expression on all cell lines.

PD1 expression on patient PBMC samples was determined by flow cytometry using anti-human PD1-APC (clone EH12.2H7, BioLegend) after overnight culture. Live cells were selected using calcein blue, AM staining (ThermoFisher) and T lymphocytes and sub-populations were identified using a cocktail of anti-human CD3-PECy5, anti-human CD4-PE, anti-human CD8-FITC antibodies (clone UCHT1; RPA-T4; RPA-T8, Biolegend) and CD62L-PerCP/Cy5.5 antibodies (clone DREG-56, BioLegend). All antibody incubations for flow cytometry were performed for 20 minutes at 4°C in phosphate buffered saline supplemented with 2% FBS. Positively stained cells were determined by gating based on fluorescence minus one (FMO) control.

Immunohistochemistry (IHC) staining and interpretation

For PD-L1 characterization of patient samples, formalin-fixed, paraffin-embedded tissue blocks from patients undergoing surgical resection at New York Presbyterian Hospital-Weill Cornell Medicine were cut into 5 µm thick sections. Consecutive slides from each tissue block were stained for hematoxylin and eosin (H&E), ICAM1 (clone G-5, Santa Cruz), PD-L1 (SP142, Spring Biosciences). Mouse lung and heart tissues were formalin-fixed, paraffin-embedded, and cut into 5 µm thick sections. IHC analysis was performed using H&E, CD3 (NCL-CD3-PD1, Leica), PD-L1 (SP142), PD1 (EPR4877(2), Abcam), and GFP (6AT316, Abcam) antibodies. Slides were scanned at a 20x magnification via an Aperio AT2 whole slide scanner (Leica Biosystems). Tumor cell distribution was evaluated in a 2.2 mm-diameter circle (10x objective field of view), and positively stained cells were quantitated using an imaging analysis software (HALO DIA) (32). An endocrine pathologist reviewed each case for consistency.

CAR T construction and transduction of T cells

ICAM1-targeted third generation CAR T constructs were engineered using either the scFv of the ICAM1-specific R6.5 monoclonal antibody or the affinity-modulated binding site of the native ligand LFA-1 (Phe-292-Ala, F292A) (33) and packaged using lentiviral plasmids as described previously (21,22). The SSTR2 gene was incorporated into CAR construct to enable whole body CAR T cell localization (23). CAR T cells were manufactured by two different methods of tissue culture versus automated CliniMACS Prodigy (Miltenyi biotec) (Supplementary Table 1). For the tissue culture method, human T cells were sequentially transduced at 24 hr after activation with CD3/CD28 Dynabeads and again 24 hr after initial transduction - each by overnight incubation. The virus titer was adjusted to obtain a transduction level of approximately 50% CAR-positive T cell. For CAR T cells used for *in vivo* studies, F292A-CAR T cells were generated with Prodigy using commercial donor leukopaks according to (31).

Effector-to-target assay

Firefly luciferase-expressing target cells (8505C, JV, HeLa, KHM-5M, and HEK293T cell lines) were plated in triplicate at a density of 5×10^3 cells per well. Cells were co-cultured with either non-transduced T cells or anti-ICAM1 CAR T cells at a 2.5:1 ratio (1.25×10^4 cells) in media containing 150 µg/mL D-luciferin (Gold Biotechnology) with or without anti-PD1 antibody (EH12.2H7, Biolegend) at a concentration of 5 µg/mL. For some experiments, AZD1480 (Selleck) was added together with T cells to inhibit JAK2 activity.

Tumor cell viability was measured periodically over 48 hours using a plate reader (TECAN Infinite M1000 PRO).

Mouse study

Eight- to ten-week old NOD-*scid*IL2Rg^{null} immunodeficient mice (NSG, Jackson Laboratory) were used for all xenograft experiments under the approval of the Institutional Animal Care and Use Committee at Weill Cornell Medicine. Systemic xenograft models were established using the fLuc-expressing 8505C ATC tumor cell line with intravenous (i.v.) injection of 0.5×10^6 cells per mouse, resulting in reliable tumor development in the lung, liver, and joints of the animals. Five days post-tumor xenograft, mice were treated with a total of 10^6 non-transduced control T cells and anti-ICAM1 CAR T cells (F292A). Cryopreserved T cells were rapidly thawed immediately prior to infusion, and injected into mice in a 100 μ L solution via tail vein injection. Selected mice were injected intraperitoneally (i.p.) with 150 μ g of anti-PD1 antibody (Biolegend clone EH12.2H7) on day five and then twice a week thereafter.

Tumor growth was tracked *in vivo* via whole-body luminescence imaging (In-Vivo Xtreme 4MP, Bruker) on a weekly basis with imaging occurring at the point of peak luminescence signal approximately 14 minutes after i.p. injection of 3 mg D-luciferin (GoldBio) per mouse. Tumor burden was quantified by integrating total luminescence flux using Bruker Analysis software.

SSTR2-expressing CAR T cells were tracked weekly *in vivo* after i.v. injection of the ¹⁸F-NOTA-octreotide radiotracer (NOTAOCT, GMP grade, ABX Pharmaceuticals) followed by PET/CT imaging within a micro-PET/CT scanner (Inveon, Siemens) (22). A known reference sample was used during imaging by including a tube containing 100 μ L of NOTAOCT (10 %ID/cm³) for quantification of NOTAOCT uptake. The %ID/cm³ values, computed relative to the counts in the reference tube, can be approximated to a standard uptake value (SUV) by dividing %ID/cm³ by four, assuming injection efficiency of 100% and 25 g of body weight. Visualization and analyses of PET/CT images were performed using Amide (<http://amide.sourceforge.net>).

Statistical Analysis

Comparison of continuous variables was performed using the Wilcoxon rank-sum test for nonparametric variables and Student's t test or ANOVA test for parametric variables. Categorical variables were compared using Fisher's exact test. Survival analysis was performed using the log-rank test. Statistical analyses were made using Stata Version 16.0 (StataCorp, College Station, TX) and Prism 8.0 (GraphPad). Statistical significance was set at two-tailed $P < 0.05$.

RESULTS

PD-L1 and ICAM1 expression correlate with PDT/ATC histology and aggressive features.

Previously, we reported that ICAM1 overexpression is a reliable marker associated with PDT and ATC (21). To determine association between ICAM1 and PD-L1 expression in

thyroid tumors, we examined both PD-L1 and ICAM1 via IHC in patients with WDPTC ($n = 19$) or PDTC/ATC ($n = 14$) (Table 1). Given the small number of PDTC samples and similarly aggressive clinical behavior between PDTC and ATC, we grouped these tumor types together and compared them to WDPTC for the statistical analysis. We used a 1% cutoff for positivity of PD-L1, a criteria previously used for melanoma (34) and head and neck squamous cell carcinoma (35). Compared to WDPTC, the PDTC or ATC tumors were more likely to be positive for PD-L1, and PD-L1 positive tumors were associated with circumferential membranous ICAM1 staining (Table 1 & Fig. 1A). We previously reported that PDTC or ATC tumors were significantly correlated with the circumferential ICAM1 expression pattern on the tumors, whereas apical ICAM1 staining has been observed in WDPTC tumors (21). Additionally, patients with PD-L1 positive tumors were more likely to be presented with locally advanced tumors and distant metastases. No significant association was observed, however, between PD-L1 expression and BRAF^{V600E} mutational status. The diffuse and rampant expression of both ICAM1 and PD-L1 on aggressive thyroid tumors suggests that targeting both molecules may boost efficacy toward PDTC and ATC.

IFN γ has been described as a major soluble factor that induces ICAM1 expression in PDTC and ATC cell lines (21). PD-L1 expression is also regulated by the IFN γ signaling pathway through JAK1 and JAK2 (36). We therefore investigated whether ICAM1 and PD-L1 expression is regulated by a common pathway in ATC. Treatment of multiple established ATC cell lines (8505C, FRO, KHM-5M) and ATC patient-derived cells (JV) with exogenous IFN γ *in vitro* resulted in a significant increase in ICAM1 expression (up to 9-fold in MFI) compared to untreated controls (Fig. 1B–1C). In 8505C and FRO, the percentages of ICAM1-positive cells increased significantly after IFN γ treatment (Supplementary Fig. 1). Similarly, treatment with IFN γ significantly upregulated PD-L1 expression in the same ATC cells, albeit to a lesser extent than ICAM1 (up to 2-fold) except for JV cells where an 11-fold increase was observed. In JV cells, the frequency of PD-L1⁺ cells increased significantly relative to untreated cells (Supplementary Fig. 1). Despite the quantitative differences in the level of IFN γ -induced ICAM1 and PD-L1 expression, the surface expression of both proteins was equally sensitive to co-treatment with the JAK2 inhibitor (JAK2i), AZD1480, which reduced expression back to basal levels (Fig. 1B–1C, Supplementary Fig. 1). In the absence of IFN γ stimulation, JAK2i did not alter either ICAM1 or PD-L1 expression, demonstrating that JAK2 is a crucial mediator of IFN γ -triggered ICAM1 and PD-L1 expression but is not required for basal surface expression within unstimulated ATC cells. This finding is further corroborated by the induction patterns of mRNA encoding interferon regulatory factor 1 (IRF1), a critical transcription factor downstream of the JAK1/2 pathway within IFN γ -treated ATC cells compared to unstimulated cells or co-treated with JAK2i (Fig. 1D). Therefore, an IFN γ signaling axis within ATC cells that requires JAK2 and drives IRF1 induction mediates expression of both ICAM1 and PD-L1. ICAM1 and PD-L1 are at least in part regulated by a common pathway in ATC, which is supported by the significant correlation between expression of both these proteins in de-differentiated thyroid cancer cells (Fig. 1).

PD1 has increased expression on CD8⁺ PBMCs in patients with PDTC/ATC.

Prior studies have shown that the frequency of PD1⁺ peripheral T cells correlates with poor prognosis for patients with gastric cancer (37), pancreatic cancer (38), and non-small cell lung cancer (39). Given the high expression of PD-L1 in PDTC/ATC tumors, we investigated whether increased PD-L1 expression in PDTC/ATC tumors is correlated with the level of PD1 expression in circulating T cells. Peripheral bloods isolated from patients (WDPTC, $n = 8$; PDTC/ATC, $n = 7$) and healthy donors ($n = 5$) were analyzed by flow cytometry for CD3, CD4, CD8, and PD1-positive T cells (Fig. 2A). The prevalence of PD1⁺ cells amongst circulating CD8⁺ T cells was low in both healthy volunteers and all patients with WDPTC (median PD1⁺/CD8⁺ T cells 7%, interquartile range (IQR) 5% - 15%) compared to significantly elevated expression in patients with PDTC/ATC tumors (median PD1⁺/CD8⁺ T cells 54%, IQR 11% - 96%) (Fig. 2B). All patients with >40% PD1 expression on peripheral blood CD8⁺ T cells presented with lung metastasis at the time of diagnosis or recurrence. However, the percentage of circulating PD1⁺/CD8⁺ T cells from patient's blood did not correlate with PD-L1 positivity in tumor (Fig. 2C), suggesting that the expression of PD1 in circulating T cells was more reflective of the degree of tumor aggressiveness rather than *in situ* PD-L1 expression in the tumor.

Co-administration of anti-PD1 antibody with ICAM1-targeted CAR T cells variably enhances *in vitro* cytotoxicity against ATC cell lines.

Next, we investigated the potential for checkpoint-mediated inhibition of ICAM1 targeting-CAR T therapy based on three key findings: (1) significant enrichment of PD-L1 on de-differentiated thyroid tumors; (2) the high level of PD1 expression in the peripheral blood of advanced thyroid cancer patients; and (3) the common upstream signaling pathway of ICAM1 and PD-L1 induction in these tumors. To investigate this, we used primary CD3⁺ T cells derived from the peripheral blood of patients with thyroid tumors (ATC, PDTC, WDPTC) with varying degrees of differentiation and commercially available healthy donor leukopaks to generate CAR T cells. T cells were transduced with one of two ICAM1-directed CAR T constructs (F292A-CAR T (labeled as mAS) (22) or R6.5-CAR T (RR) (21)), which were previously shown to enable efficient T cell-mediated lysis of ICAM1-expressing ATC cell lines. The established ATC cell line 8505C (intermediate ICAM1/high PD-L1), ATC patient-derived cell line JV (high ICAM1/intermediate PD-L1), and control cell lines, 293T (low ICAM1/low PD-L1) and HeLa (high ICAM1/intermediate PD-L1) were chosen to represent various expression profiles of PD-L1 and ICAM1 (Fig. 3A). ATC cells had significantly lower surface expression of PD-L2 (PDCD1LG2) (40), another ligand of PD1, compared to PD-L1 (Fig. 3A).

The cytotoxic properties of ICAM1-CAR T cell batches generated with T cells from WDTC, PDPTC, or ATC patients as a representative of thyroid cancer with gradual loss of differentiation status were examined (Fig. 3B & Supplementary Table 1). The baseline efficacy of ICAM1-CAR T cells was demonstrated by the lysis of approximately 50% of the 8505C cell line after co-culture at a 2.5:1 effector: target (E:T) ratio. The time required to achieve 50% lysis varied between 18 to 48 hours depending on the donor blood used for CAR T manufacturing. To evaluate the effect of neutralizing PD1-signalling, the ability of ICAM-1 CAR T cells to lyse ATC cell lines in combination with anti-PD1 antibody

treatment *in vitro* was compared to lysis mediated by ICAM-1 CAR T cells alone (Fig. 3C). Compared to ICAM1-CAR T alone, the cytotoxicity of ICAM1-CAR T cells generated with ATC and WDPTC patients was significantly enhanced when anti-PD1 antibody was supplemented to ATC target cell lines. Overall, two out of four patient donor ICAM1-CAR T cell batches showed significant improvement in their ability to eradicate co-cultured target ATC cells when anti-PD1 antibody was supplemented to the media (Supplementary Table 1). Addition of anti-PD1 antibody to non-transduced T (NT) cells did not affect cell behavior in the same settings. However, donor T cell PD1 expression level or donor thyroid tumor histopathological type (e.g. WDPTC vs. PDPTC and ATC) did not correlate with *in vitro* responders to anti-PD1 treatment (Supplementary Table 1).

Anti-PD1 therapy in combination with ICAM1-CAR T treatment confers a survival advantage over ICAM1-CAR T alone in a preclinical murine model.

A metastatic model of human ATC was created by systemic engraftment of the 8505C- β Luc/GFP cell line into NSG mice. These mice were later treated with ICAM1-CAR T cells manufactured from three commercial donor leukopaks derived from healthy donors (CAR T-1, CAR T-2, CAR T-3) with different percentages of PD1-expressing CD8⁺ T cells but similar CAR T transduction frequencies (Fig. 4A and Supplementary Table 1). The CAR T manufacturing preserved the ratio of CD4:CD8 in CAR T cells of each donor leukopak (Fig. 4A and Supplementary Fig. 2A). The CAR T transduction frequencies in live T cells were determined by measuring the expression of the myc peptide tag that is fused to CAR at the N-terminal. The expression of SSTR2, which is co-expressed by a ribosome skipping sequence P2A within the CAR expression cassette was also confirmed to validate T cell trafficking by PET/CT (31). *In vitro* E:T experiments using CAR T cell batches manufactured from each of the three donors demonstrated cytotoxicity against target ATC cells (Fig. 4B). However, enhanced killing with anti-PD1 antibody was observed with CAR T-1 only. Next, the three CAR T cell batches were tested for activity *in vivo* with or without PD1 blockade. Mice were administered with CAR T cells five days after xenograft with 8505C cells; PD1 cohort additionally received twice-weekly injections of 150 μ g of anti-PD1 antibody for 8 weeks. Whole body luminescence imaging showed that all three donor CAR T cell batches reduced the tumor burden drastically in treated animals compared to mice left untreated or treated with NT cells (Fig. 4C). However, when the rates of *in vivo* tumor luminescence reduction mediated by each donor CAR batch were compared, a disparate tumor lytic response was observed. Donor CAR T-1 cells, which displayed the highest level of PD1 expression and were responsive to anti-PD1 treatment *in vitro* (Fig. 4A), also exhibited an enhanced tumor lytic response when anti-PD1 antibody was administered together with CAR T cells: the CAR T-1 and anti-PD1 antibody combination demonstrated significantly enhanced tumor burden reduction when compared to the effect of CAR T-1 alone at 3–4 weeks post-xenograft, ($P < 0.01$) (Fig. 4C–D & Supplementary Table 1). Interestingly, CAR T-1 retained the highest percentage of CD62L^{low}CD4⁺ T cell subset population compared to other donor CAR T cells (Supplementary Fig. 2B). In non-small lung cancer patients, the frequency of CD62L^{low}CD4⁺ T cells has been correlated with long-term responders to anti-PD1 therapy (41). Overall, all mice receiving ICAM1-CAR T cells and anti-PD1 antibody together showed a significant survival benefit compared to mice treated with ICAM1-CAR T only (Fig. 4E). The additive benefit of anti-PD1 therapy to

CAR T cells was more apparent in an *in vivo* condition with a long-term follow-up period. The combined treatment of ICAM1-CAR T cells and anti-PD1 antibody also showed improvement in survival in xenografts with KHM-5M, another ATC line with ICAM1 expression (Figure 1B), compared to treatment with ICAM1-CAR T cells alone (Supplementary Figure 3).

Anti-PD1 antibody reduces the peak expansion of ICAM1-CAR T cells and facilitates subsequent contraction at the tumor site.

ICAM1-specific CAR T cells co-express SSTR2, which upon injection of a positron-emitting SSTR2-specific tracer, ¹⁸F-NOTA-Octreotide (NOTAOCT), enables whole-body tracking and localization of CAR T cells by PET/CT (Fig. 5A) (22). Previously, we were able to detect multiple phases of CAR T cell activity in correlation with tumor clearance, characterized by rapid expansion and contraction of T cells at metastatic thyroid tumor sites *in vivo* (22,23). In the current study, the peak or near-peak expansion of ICAM1-targeting CAR T cells were detected in the lungs three weeks after tumor injection (Fig. 5A). To assess whether CAR T cell temporal kinetics was altered by anti-PD1 antibody, we quantified the uptake of NOTAOCT tracers in 8505C-xenografted mice that were treated with different treatments (Fig. 5B). This analysis revealed that anti-PD1 antibody significantly reduced CAR T cell expansion at its peak (week 3–4) and contraction phase (week 5 post-xenograft). Lower expansion of CAR T cells in mice co-treated with anti-PD1 antibody was likely due to a faster elimination of tumor cells, avoiding a prolonged expansion of T cells against delayed clearance of tumor (Fig. 5B and 4C).

Anti-PD1 antibody restricts the activity and proliferation of ICAM1-CAR T cells at tumor cells.

To examine the effect of anti-PD1 antibody on CAR T cells at the cellular levels, we then analyzed consecutive lung sections from 8505C xenografted mice by IHC. The number of tumor-infiltrating T cells with respect to tumor cells for the different treatment groups was compared using digital image analysis (32) (Fig. 5C). The 3-week post xenograft (which is about 2-week post-CAR T treatment) was chosen as an approximate time point for maximal tumor lysis in both the CAR T alone and CAR T/anti-PD1 treatment groups. Lung tissue sections from 8505c-xenografted mice treated with CAR T cells demonstrated a marked reduction in tumor burden and increase in a number of T cell clusters (Fig. 5C–E). Dual treatment with anti-PD1 antibody and ICAM1-CAR T-1 cells revealed a further reduction in the number of tumor cells (Fig. 5E). Of the lung tumor sections that stained positive for tumor cells, specific co-localization of CD3⁺ T cells and GFP⁺ tumor cells were observed both for CAR T with or without PD1. Close examination, however, revealed that PD1 treatment led to an increased number of T cells restricted to at and in the vicinity of the remaining GFP⁺ tumor cells compared to CAR T distribution without PD1 (Fig. 5E). This result may indicate that anti-PD1 antibody treatment curtailed excessive expansion of CAR T cells by augmenting cytotoxicity and proliferation capacity of CAR T cells limited to interaction with tumor cells. In comparison, xenografted mice treated with NT cells displayed the highest tumor burden as shown by the abundance of GFP⁺ tumor cells remaining in the lung (Fig. 5C–E). The additional administration of anti-PD1 antibody to mice treated with NT cells significantly elevated the density of T cells in the lung; however,

T cell expansion was found to be non-specific to T cell interaction with tumor cells (Fig. 5D).

Anti-PD1 antibody relieves the inhibitory effects of PD1 induction in CAR T cells.

As the addition of anti-PD1 antibody improves ICAM1-directed tumor lysis by CAR T *in vitro* and *in vivo*, we investigated whether this benefit is specific to the activity of the CAR T cells but not to non-tumor directed T cells. Compared to NT cells, PD1 expression was significantly induced in ICAM1-CAR T cells only when exposed to ICAM1-positive 8505C, JV, and HeLa cells compared to ICAM1-negative 293T cells (Fig. 6A–B). JAK2i abrogated PD1 induction in ICAM1-CAR T cells, implicating that PD1 is induced through the IFN γ -JAK2 signaling pathway.

We further investigated PD1 expression in xenografts treated with ICAM1-CAR T-1 cells. In order to enumerate the density of tumor-infiltrating T cells, we analyzed the same high density tumor areas for PD1 and CD3 in the consecutive slides of the lung sections. At 3-week post-xenograft (2-week post-CAR T injection), the number of PD1⁺ T cells was significantly increased in the CAR T cohort relative to NT treatment group (Fig. 6C). The fraction of PD1⁺ T cells was approximately 17% of CD3⁺ T cells, whereas 1% of NT cells were PD1⁺ (Treatment cohorts with anti-PD1 antibody were not analyzed for PD1⁺ due to epitope overlap or steric hindrance between the treatment antibody and IHC antibody (42)). In contrast, we found that the PD-L1⁺ cell density was significantly reduced in CAR T-treated mice compared to NT-treated mice (Fig. 6D). The majority of the remaining GFP⁺ tumor cells in CAR T-treatment group were also PD-L1⁺, whereas combination treatment with CAR T cells and anti-PD1 antibody eliminated most PD-L1 high cluster of tumor cells (Fig. 6D).

DISCUSSION

Both CAR T and immune checkpoint therapies are therapeutic strategies under clinical development for patients with advanced thyroid cancers. Here we demonstrated that dual targeting of ICAM1 and PD-L1 by combined administration of ICAM1-targeting CAR T cells and anti-PD1 antibody showed enhanced therapeutic effects in an ATC mouse model, marked by increased expansion and localization of T cells at cluster of tumor cells, reduced tumor burden, and improved overall survival. Clinical specimens in our study also showed that PDTC/ATC tumor had significantly increased expression of both PD-L1 and ICAM1, and peripheral T cells from advanced thyroid cancer patients showed that patients with PDTC/ATC exhibited upregulated PD1 expression. These findings in clinical specimens and animal models in our study supports the potential benefits of PD1 blockade therapy in combination with ICAM1-targeting CAR T cells against advanced thyroid cancer.

Our study provides an important insight into the inhibitory interaction between PD-L1 and PD1 that is prominent in advanced thyroid cancers (14–16). Although PD1 expression on tumor-infiltrating T cells correlates with unfavorable prognosis in many human tumors, less is known about PD1 expression in peripheral T cells and its functional characteristics (43,44). We found significantly elevated PD1 expression in peripheral blood CD8⁺ T cells from the advanced thyroid cancer patients with lung metastasis at the time of diagnosis or

recurrence. However, the high frequency of PD1⁺CD8⁺ T cells in these patients was not correlated with the PD-L1 positivity in the tumor biopsy. Since tumor PD-L1 expression is known to be heterogeneous and inducible by different stimuli, IHC analysis in one area of the tumor may be inadequate to fully capture PD-L1 expression across entire tumor mass. Further investigation of PD1⁺ peripheral CD8⁺ cells with a larger sample size will be necessary to assess the value of PD1 positivity as a prognostic biomarker in advanced thyroid tumors, as has been shown in pancreatic (38) and gastric cancers (37).

The potential benefit of targeting both ICAM-1 and immune checkpoint is further corroborated by our studies revealing a common pathway that regulates ICAM1 and PD-L1 induction. We found that PDTC and ATC cells express high levels of both ICAM1 and PD-L1 at the cell membrane, and upon IFN γ stimulation induced expression of PD-L1 and ICAM1 in a JAK2-dependent manner. IFN γ binds to the interferon receptor, which activates a rapid and transient JAK and STAT signaling and induces interferon-stimulated gene (45). Dysregulation of IFN γ -JAK2 pathway has been uncovered as a key mechanism for tumor cells to evade the native adaptive immune system (46,47). IRF1 is a crucial transcription factor mediating the IFN γ -induced transcription of cellular genes. We have shown that inhibition of JAK2 lowers the *IRF1* transcript level and surface expression of PD-L1 and ICAM1 in IFN γ -treated ATC cell lines. We demonstrated that PD1 expression in CAR T cells is also induced in a JAK2-dependent fashion when CAR T cells are engaged in target cell lysis. Coordinated molecular regulation of PD-L1 and ICAM1 in tumors and PD1 in T cells supports our hypothesis that targeting both ICAM1 and PD1 in CAR T cells can deliver more effective and specific methods to control advanced thyroid tumor growth.

Our study demonstrated a previously unappreciated, critical role for PD1 blockade in augmenting the CAR T safety profile. Previously, modulation of PD1 signaling has been shown to provide benefits in CAR T efficacy within other types of preclinical solid tumor models (44,48–51) and, potentially, in subsets of patients with B-cell lineage malignancies (26). Our analyses of whole-body PET/CT and IHC on the tumor tissues showed that PD1 blockade therapy increased the density of the tumor-targeting ICAM1-CAR T cells more restricted to the interaction with tumor cells, resulting in more efficient elimination of tumor and diminished expansion away from the tumor cells. The impact of anti-PD1 antibody on CAR T cells at the cellular levels resulted in faster tumor elimination and diminished CAR T expansion in the body. Additional analyses at an earlier timepoint would be helpful to capture initial antigen-driven CAR T expansion and to understand whether anti-PD1 antibody has the same effect on the CAR T cell interaction with the tumor cells. Dual treatment of CAR T cells and anti-PD1 antibody were found to be effective in removing the PD-L1⁺ tumor colonies that were resistant to CAR T treatment alone. Our findings also implicate that strategies to inhibit PD1 signaling in CAR T therapy may reduce off-tumor toxicities of CAR T cells.

ATC exhibits features, such as a high mutation burden (2,8,52), greater density of CD8⁺ TILs (15), and tumor PD-L1 positivity (14,16), that cumulatively would indicate sensitivity to immune checkpoint therapies. However, early clinical studies reported that fewer than 20% of ATC patients exhibited limited responses to this therapy (53). These studies illustrate that additional targeting strategies are needed to make PD1 or PD-L1 blockade therapy to

achieve higher clinical response against advanced thyroid cancers. We noted that CAR T-1 cells that displayed over 40% PD1 positivity and had expanded poorly against ATC showed improved effector function *in vivo* when anti-PD1 was administered. In addition to exhibiting high PD1⁺CD8⁺ T cell frequency, this donor leukopak had elevated percentage of CD62L^{low}CD4⁺ T cells in the periphery. A recent study indicates that this population that is enriched for Th1 cell pool contributes to durable antitumor response in response to anti-PD1 therapy (41). Understanding whether cytotoxic CD8⁺ and CD4⁺ Th1 cell pools within CAR T cells upon tumor contact would induce the IFN γ signaling axis will be important to predict advanced thyroid cancer patients that would benefit from PD1 blockade combination.

In this study, we investigated the tumor targeting ability of CAR T cells in immunodeficient mice using human tumor xenografts. Therefore, our study is limited in its ability to predict clinical efficacy of combined treatments of ICAM1-CAR T and anti-PD1 antibody in a natural advanced thyroid tumor microenvironment in human tumors. Advanced thyroid cancers, in particular ATC, are known to be associated with an increased density of M2 tumor associated macrophages with an immunosuppressive phenotype (14,54,55). ICAM1 is also a marker for inflammation, and chronic inflammation has long been known to promote an immunosuppressive tumor microenvironment and tumor development (56). ICAM1 expression may be induced by proinflammatory cytokines such as IFN γ , TNF α , and IL1 β in endothelial cells and other cell types (57–60). Optimizing strategies to limit off target toxicity, such as retaining cytotoxicity against the tumors with the highest ICAM1 expression but sparing healthy normal tissue, will be crucial to bringing ICAM1-CAR T into a clinical setting. Ultimately, it will be necessary to tailor CAR T cell treatment and adjuvant immune inhibitory blockade to the patients' tumor and T cell characteristics to enhance treatment potency and limit toxicity. Determining the characteristics of patient's T cells that respond to combination therapy of CAR T cells and anti-PD antibody will help to identify those patients who are most likely to respond to this combination therapy.

In conclusion, we have found that advanced thyroid cancer patients exhibit elevated expression of IFN γ -inducible ICAM1 and PD-L1 in tumors and PD1 in peripheral CD8⁺ T cells. Directed targeting of CAR T cells against ICAM1, a membrane antigen abundantly expressed in advanced thyroid cancers, further enhances the expression of the target antigen ICAM1 as well as PD-L1 in the ATC tumor cells and PD1 in the CAR T cells via the IFN γ -JAK2 signaling pathway. We further demonstrated that dual targeting of both ICAM1 and PD-L1 in a mouse model of ATC can improve survival with potential benefit to safety (proposed model in Supplementary Fig. 4). These findings provide the basis for translational relevance of dual treatment employing ICAM1-targeting CAR T cells and PD1/PD-L1 blockade therapy.

Supplementary Material

Refer to Web version on PubMed Central for supplementary material.

Acknowledgments:

This working is supported by the Bite me Cancer-American Thyroid Association (ID-2016-052) (to I.M. Min), New York State Department of Health (DOH-01-C32575GG-34500) (to I.M. Min), Emerson Collective Cancer Research Fund (ECCRF 191824-01) (to I.M. Min), NCI R01 CA217059 (to M.M. Jin), and Dancer's Care Foundation (T.J. Fahey). The authors would like to acknowledge the support of the Translational Research, Clinical & Translational Science Center (1-UL1-TR002384-01), Flow cytometry Core, and the CITI Biomedical Imaging Center, all at Weill Cornell Medicine.

References

1. Cabanillas ME, McFadden DG, Durante C. Thyroid cancer. *Lancet* 2016;388(10061):2783–95 doi 10.1016/S0140-6736(16)30172-6. [PubMed: 27240885]
2. Landa I, Ibrahimipasic T, Boucai L, Sinha R, Knauf JA, Shah RH, et al. Genomic and transcriptomic hallmarks of poorly differentiated and anaplastic thyroid cancers. *J Clin Invest* 2016;126(3):1052–66 doi 10.1172/JCI85271. [PubMed: 26878173]
3. Smallridge RC, Ain KB, Asa SL, Bible KC, Brierley JD, Burman KD, et al. American Thyroid Association guidelines for management of patients with anaplastic thyroid cancer. *Thyroid* 2012;22(11):1104–39 doi 10.1089/thy.2012.0302. [PubMed: 23130564]
4. Xu B, Ghossein R. Genomic Landscape of poorly Differentiated and Anaplastic Thyroid Carcinoma. *Endocr Pathol* 2016;27(3):205–12 doi 10.1007/s12022-016-9445-4. [PubMed: 27372303]
5. Savvides P, Nagaiah G, Lavertu P, Fu P, Wright JJ, Chapman R, et al. Phase II trial of sorafenib in patients with advanced anaplastic carcinoma of the thyroid. *Thyroid* 2013;23(5):600–4 doi 10.1089/thy.2012.0103. [PubMed: 23113752]
6. Iniguez-Ariza NM, Ryder MM, Hilger CR, Bible KC. Salvage Lenvatinib Therapy in Metastatic Anaplastic Thyroid Cancer. *Thyroid* 2017;27(7):923–7 doi 10.1089/thy.2016.0627. [PubMed: 28471306]
7. Subbiah V, Kreitman RJ, Wainberg ZA, Cho JY, Schellens JHM, Soria JC, et al. Dabrafenib and Trametinib Treatment in Patients With Locally Advanced or Metastatic BRAF V600-Mutant Anaplastic Thyroid Cancer. *J Clin Oncol* 2018;36(1):7–13 doi 10.1200/JCO.2017.73.6785. [PubMed: 29072975]
8. Kunstman JW, Juhlin CC, Goh G, Brown TC, Stenman A, Healy JM, et al. Characterization of the mutational landscape of anaplastic thyroid cancer via whole-exome sequencing. *Hum Mol Genet* 2015;24(8):2318–29 doi 10.1093/hmg/ddu749. [PubMed: 25576899]
9. Herbst RS, Baas P, Kim DW, Felip E, Perez-Gracia JL, Han JY, et al. Pembrolizumab versus docetaxel for previously treated, PD-L1-positive, advanced non-small-cell lung cancer (KEYNOTE-010): a randomised controlled trial. *Lancet* 2016;387(10027):1540–50 doi 10.1016/S0140-6736(15)01281-7. [PubMed: 26712084]
10. Fehrenbacher L, Spira A, Ballinger M, Kowanzetz M, Vansteenkiste J, Mazieres J, et al. Atezolizumab versus docetaxel for patients with previously treated non-small-cell lung cancer (POPLAR): a multicentre, open-label, phase 2 randomised controlled trial. *Lancet* 2016;387(10030):1837–46 doi 10.1016/S0140-6736(16)00587-0. [PubMed: 26970723]
11. Carretero-Gonzalez A, Lora D, Ghanem I, Zugazagoitia J, Castellano D, Sepulveda JM, et al. Analysis of response rate with ANTI PD1/PD-L1 monoclonal antibodies in advanced solid tumors: a meta-analysis of randomized clinical trials. *Oncotarget* 2018;9(9):8706–15 doi 10.18632/oncotarget.24283. [PubMed: 29492229]
12. LaFleur MW, Muroyama Y, Drake CG, Sharpe AH. Inhibitors of the PD-1 Pathway in Tumor Therapy. *J Immunol* 2018;200(2):375–83 doi 10.4049/jimmunol.1701044. [PubMed: 29311378]
13. Sharma P, Allison JP. The future of immune checkpoint therapy. *Science* 2015;348(6230):56–61 doi 10.1126/science.aaa8172. [PubMed: 25838373]
14. Zwaenepoel K, Jacobs J, De Meulenaere A, Silence K, Smits E, Siozopoulou V, et al. CD70 and PD-L1 in anaplastic thyroid cancer - promising targets for immunotherapy. *Histopathology* 2017;71(3):357–65 doi 10.1111/his.13230. [PubMed: 28383817]
15. Bastman JJ, Serracino HS, Zhu Y, Koenig MR, Mateescu V, Sams SB, et al. Tumor-Infiltrating T Cells and the PD-1 Checkpoint Pathway in Advanced Differentiated and Anaplastic Thyroid

- Cancer. *J Clin Endocrinol Metab* 2016;101(7):2863–73 doi 10.1210/jc.2015-4227. [PubMed: 27045886]
16. Ahn S, Kim TH, Kim SW, Ki CS, Jang HW, Kim JS, et al. Comprehensive screening for PD-L1 expression in thyroid cancer. *Endocr Relat Cancer* 2017;24(2):97–106 doi 10.1530/ERC-16-0421. [PubMed: 28093480]
 17. Mehnert JM, Varga A, Brose MS, Aggarwal RR, Lin CC, Prawira A, et al. Safety and antitumor activity of the anti-PD-1 antibody pembrolizumab in patients with advanced, PD-L1-positive papillary or follicular thyroid cancer. *BMC Cancer* 2019;19(1):196 doi 10.1186/s12885-019-5380-3. [PubMed: 30832606]
 18. Wirth LJE E; Capdevila J; Paz-Ares LG; Lin C; Taylor MH; Ramlau R; Butler M; Delord J; Horvath Z; Gelderblom H; Ascierto PA; Fasolo A; Führer D; Wu H; Bostel G; Cameron S; Faris JE; and Varga AI Phase I/II study of spartalizumab (PDR001), an anti-PD1 mAb, in patients with anaplastic thyroid cancer. *Journal of Clinical Oncology* 2018;36:6024-.
 19. Hubbard AK, Rothlein R. Intercellular adhesion molecule-1 (ICAM-1) expression and cell signaling cascades. *Free Radic Biol Med* 2000;28(9):1379–86 doi 10.1016/s0891-5849(00)00223-9. [PubMed: 10924857]
 20. Buitrago D, Keutgen XM, Crowley M, Filicori F, Aldailami H, Hoda R, et al. Intercellular adhesion molecule-1 (ICAM-1) is upregulated in aggressive papillary thyroid carcinoma. *Ann Surg Oncol* 2012;19(3):973–80 doi 10.1245/s10434-011-2029-0. [PubMed: 21879273]
 21. Min IM, Shevlin E, Vedvyas Y, Zaman M, Wyrwas B, Scognamiglio T, et al. CAR T Therapy Targeting ICAM-1 Eliminates Advanced Human Thyroid Tumors. *Clin Cancer Res* 2017;23(24):7569–83 doi 10.1158/1078-0432.CCR-17-2008. [PubMed: 29025766]
 22. Park S, Shevlin E, Vedvyas Y, Zaman M, Park S, Hsu YS, et al. Micromolar affinity CAR T cells to ICAM-1 achieves rapid tumor elimination while avoiding systemic toxicity. *Sci Rep* 2017;7(1):14366 doi 10.1038/s41598-017-14749-3. [PubMed: 29085043]
 23. Vedvyas Y, Shevlin E, Zaman M, Min IM, Amor-Coarasa A, Park S, et al. Longitudinal PET imaging demonstrates biphasic CAR T cell responses in survivors. *JCI Insight* 2016;1(19):e90064 doi 10.1172/jci.insight.90064. [PubMed: 27882353]
 24. Beatty GL, Moon EK. Chimeric antigen receptor T cells are vulnerable to immunosuppressive mechanisms present within the tumor microenvironment. *Oncoimmunology* 2014;3(11):e970027 doi 10.4161/21624011.2014.970027. [PubMed: 25941599]
 25. Moon EK, Wang LC, Dolfi DV, Wilson CB, Ranganathan R, Sun J, et al. Multifactorial T-cell hypofunction that is reversible can limit the efficacy of chimeric antigen receptor-transduced human T cells in solid tumors. *Clin Cancer Res* 2014;20(16):4262–73 doi 10.1158/1078-0432.CCR-13-2627. [PubMed: 24919573]
 26. Rafiq S, Hackett CS, Brentjens RJ. Engineering strategies to overcome the current roadblocks in CAR T cell therapy. *Nat Rev Clin Oncol* 2020;17(3):147–67 doi 10.1038/s41571-019-0297-y. [PubMed: 31848460]
 27. June CH, O'Connor RS, Kawalekar OU, Ghassemi S, Milone MC. CAR T cell immunotherapy for human cancer. *Science* 2018;359(6382):1361–5 doi 10.1126/science.aar6711. [PubMed: 29567707]
 28. June CH, Sadelain M. Chimeric Antigen Receptor Therapy. *N Engl J Med* 2018;379(1):64–73 doi 10.1056/NEJMra1706169. [PubMed: 29972754]
 29. Brown CE, Mackall CL. CAR T cell therapy: inroads to response and resistance. *Nat Rev Immunol* 2019;19(2):73–4 doi 10.1038/s41577-018-0119-y. [PubMed: 30631206]
 30. Martinez M, Moon EK. CAR T Cells for Solid Tumors: New Strategies for Finding, Infiltrating, and Surviving in the Tumor Microenvironment. *Front Immunol* 2019;10:128 doi 10.3389/fimmu.2019.00128. [PubMed: 30804938]
 31. Vedvyas Y, McCloskey JE, Yang Y, Min IM, Fahey TJ, Zarnegar R, et al. Manufacturing and preclinical validation of CAR T cells targeting ICAM-1 for advanced thyroid cancer therapy. *Sci Rep* 2019;9(1):10634 doi 10.1038/s41598-019-46938-7. [PubMed: 31337787]
 32. McIntire PJ, Zhong E, Patel A, Khani F, D'Alfonso TM, Chen Z, et al. Hotspot enumeration of CD8+ tumor-infiltrating lymphocytes using digital image analysis in triple-negative breast cancer

- yields consistent results. *Hum Pathol* 2019;85:27–32 doi 10.1016/j.humpath.2018.10.014. [PubMed: 30381263]
33. Jin M, Song G, Carman CV, Kim YS, Astrof NS, Shimaoka M, et al. Directed evolution to probe protein allostery and integrin I domains of 200,000-fold higher affinity. *Proc Natl Acad Sci U S A* 2006;103(15):5758–63 doi 10.1073/pnas.0601164103. [PubMed: 16595626]
 34. Daud AI, Wolchok JD, Robert C, Hwu WJ, Weber JS, Ribas A, et al. Programmed Death-Ligand 1 Expression and Response to the Anti-Programmed Death 1 Antibody Pembrolizumab in Melanoma. *J Clin Oncol* 2016;34(34):4102–9 doi 10.1200/JCO.2016.67.2477. [PubMed: 27863197]
 35. Chow LQM, Haddad R, Gupta S, Mahipal A, Mehra R, Tahara M, et al. Antitumor Activity of Pembrolizumab in Biomarker-Unselected Patients With Recurrent and/or Metastatic Head and Neck Squamous Cell Carcinoma: Results From the Phase Ib KEYNOTE-012 Expansion Cohort. *J Clin Oncol* 2016;34(32):3838–45 doi 10.1200/JCO.2016.68.1478. [PubMed: 27646946]
 36. Garcia-Diaz A, Shin DS, Moreno BH, Saco J, Escuin-Ordinas H, Rodriguez GA, et al. Interferon Receptor Signaling Pathways Regulating PD-L1 and PD-L2 Expression. *Cell Rep* 2017;19(6):1189–201 doi 10.1016/j.celrep.2017.04.031. [PubMed: 28494868]
 37. Saito H, Shimizu S, Kono Y, Murakami Y, Shishido Y, Miyatani K, et al. PD-1 Expression on Circulating CD8(+) T-Cells as a Prognostic Marker for Patients With Gastric Cancer. *Anticancer Res* 2019;39(1):443–8 doi 10.21873/anticancer.13132. [PubMed: 30591493]
 38. Shen T, Zhou L, Shen H, Shi C, Jia S, Ding GP, et al. Prognostic value of programmed cell death protein 1 expression on CD8+ T lymphocytes in pancreatic cancer. *Sci Rep* 2017;7(1):7848 doi 10.1038/s41598-017-08479-9. [PubMed: 28798308]
 39. Arrieta O, Montes-Servin E, Hernandez-Martinez JM, Cardona AF, Casas-Ruiz E, Crispin JC, et al. Expression of PD-1/PD-L1 and PD-L2 in peripheral T-cells from non-small cell lung cancer patients. *Oncotarget* 2017;8(60):101994–2005 doi 10.18632/oncotarget.22025. [PubMed: 29254220]
 40. Keir ME, Liang SC, Guleria I, Latchman YE, Qipo A, Albacker LA, et al. Tissue expression of PD-L1 mediates peripheral T cell tolerance. *J Exp Med* 2006;203(4):883–95 doi 10.1084/jem.20051776. [PubMed: 16606670]
 41. Kagamu H, Kitano S, Yamaguchi O, Yoshimura K, Horimoto K, Kitazawa M, et al. CD4(+) T-cell Immunity in the Peripheral Blood Correlates with Response to Anti-PD-1 Therapy. *Cancer Immunol Res* 2020;8(3):334–44 doi 10.1158/2326-6066.CIR-19-0574. [PubMed: 31871122]
 42. Kleffel S, Posch C, Barthel SR, Mueller H, Schlapbach C, Guenova E, et al. Melanoma Cell-Intrinsic PD-1 Receptor Functions Promote Tumor Growth. *Cell* 2015;162(6):1242–56 doi 10.1016/j.cell.2015.08.052. [PubMed: 26359984]
 43. Popovic A, Jaffee EM, Zaidi N. Emerging strategies for combination checkpoint modulators in cancer immunotherapy. *J Clin Invest* 2018;128(8):3209–18 doi 10.1172/JCI120775. [PubMed: 30067248]
 44. Sharpe AH, Pauken KE. The diverse functions of the PD1 inhibitory pathway. *Nat Rev Immunol* 2018;18(3):153–67 doi 10.1038/nri.2017.108. [PubMed: 28990585]
 45. Ivashkiv LB. IFN γ : signalling, epigenetics and roles in immunity, metabolism, disease and cancer immunotherapy. *Nat Rev Immunol* 2018;18(9):545–58 doi 10.1038/s41577-018-0029-z. [PubMed: 29921905]
 46. Zaretsky JM, Garcia-Diaz A, Shin DS, Escuin-Ordinas H, Hugo W, Hu-Lieskovan S, et al. Mutations Associated with Acquired Resistance to PD-1 Blockade in Melanoma. *N Engl J Med* 2016;375(9):819–29 doi 10.1056/NEJMoa1604958. [PubMed: 27433843]
 47. Gao J, Shi LZ, Zhao H, Chen J, Xiong L, He Q, et al. Loss of IFN- γ Pathway Genes in Tumor Cells as a Mechanism of Resistance to Anti-CTLA-4 Therapy. *Cell* 2016;167(2):397–404 e9 doi 10.1016/j.cell.2016.08.069. [PubMed: 27667683]
 48. Suarez ER, Chang de K, Sun J, Sui J, Freeman GJ, Signoretti S, et al. Chimeric antigen receptor T cells secreting anti-PD-L1 antibodies more effectively regress renal cell carcinoma in a humanized mouse model. *Oncotarget* 2016;7(23):34341–55 doi 10.18632/oncotarget.9114. [PubMed: 27145284]

49. Rafiq S, Yeku OO, Jackson HJ, Purdon TJ, van Leeuwen DG, Drakes DJ, et al. Targeted delivery of a PD-1-blocking scFv by CAR-T cells enhances anti-tumor efficacy in vivo. *Nat Biotechnol* 2018;36(9):847–56 doi 10.1038/nbt.4195. [PubMed: 30102295]
50. Liu X, Ranganathan R, Jiang S, Fang C, Sun J, Kim S, et al. A Chimeric Switch-Receptor Targeting PD1 Augments the Efficacy of Second-Generation CAR T Cells in Advanced Solid Tumors. *Cancer Res* 2016;76(6):1578–90 doi 10.1158/0008-5472.CAN-15-2524. [PubMed: 26979791]
51. Cherkassky L, Morello A, Villena-Vargas J, Feng Y, Dimitrov DS, Jones DR, et al. Human CAR T cells with cell-intrinsic PD-1 checkpoint blockade resist tumor-mediated inhibition. *J Clin Invest* 2016;126(8):3130–44 doi 10.1172/JCI83092. [PubMed: 27454297]
52. Giannini R, Moretti S, Ugolini C, Macerola E, Menicali E, Nucci N, et al. Immune Profiling of Thyroid Carcinomas Suggests the Existence of Two Major Phenotypes: an ATC-like and a PDTC-like. *J Clin Endocrinol Metab* 2019 doi 10.1210/jc.2018-01167.
53. Naoum GE, Morkos M, Kim B, Arafat W. Novel targeted therapies and immunotherapy for advanced thyroid cancers. *Mol Cancer* 2018;17(1):51 doi 10.1186/s12943-018-0786-0. [PubMed: 29455653]
54. Ryder M, Ghossein RA, Ricarte-Filho JC, Knauf JA, Fagin JA. Increased density of tumor-associated macrophages is associated with decreased survival in advanced thyroid cancer. *Endocr Relat Cancer* 2008;15(4):1069–74 doi 10.1677/ERC-08-0036. [PubMed: 18719091]
55. Schurch CM, Roelli MA, Forster S, Wasmer MH, Bruhl F, Maire RS, et al. Targeting CD47 in Anaplastic Thyroid Carcinoma Enhances Tumor Phagocytosis by Macrophages and Is a Promising Therapeutic Strategy. *Thyroid* 2019;29(7):979–92 doi 10.1089/thy.2018.0555. [PubMed: 30938231]
56. Shalpour S, Karin M. Immunity, inflammation, and cancer: an eternal fight between good and evil. *J Clin Invest* 2015;125(9):3347–55 doi 10.1172/JCI80007. [PubMed: 26325032]
57. Smith CW, Rothlein R, Hughes BJ, Mariscalco MM, Rudloff HE, Schmalstieg FC, et al. Recognition of an endothelial determinant for CD 18-dependent human neutrophil adherence and transendothelial migration. *J Clin Invest* 1988;82(5):1746–56 doi 10.1172/JCI113788. [PubMed: 2903180]
58. Mickelson JK, Kukielka G, Bravenec JS, Mainolfi E, Rothlein R, Hawkins HK, et al. Differential expression and release of CD54 induced by cytokines. *Hepatology* 1995;22(3):866–75. [PubMed: 7657294]
59. Lu Y, Yu T, Liang H, Wang J, Xie J, Shao J, et al. Nitric oxide inhibits hetero-adhesion of cancer cells to endothelial cells: restraining circulating tumor cells from initiating metastatic cascade. *Sci Rep* 2014;4:4344 doi 10.1038/srep04344. [PubMed: 24614329]
60. Pober JS, Gimbrone MA Jr., Lapierre LA, Mendrick DL, Fiers W, Rothlein R, et al. Overlapping patterns of activation of human endothelial cells by interleukin 1, tumor necrosis factor, and immune interferon. *J Immunol* 1986;137(6):1893–6. [PubMed: 3091693]

Translational Relevance

Patients with advanced thyroid cancers have a poor response to known systemic therapies with the disease-specific mortality rates that range between 40 – 100%. Early clinical trials indicate that these tumors do not respond well to immune checkpoint therapies. We analyzed tumor and blood samples from the patients with advanced thyroid cancers, and found that both ICAM1 and PD-L1 were overexpressed in tumor cells and PD1 expression was significantly high in the peripheral CD8⁺ T cells. In a xenograft mouse model of anaplastic thyroid cancer, a dual treatment with ICAM1-targeting CAR T cells and anti-PD1 antibody showed superior efficacy in tumor burden reduction and enhanced survival when compared to CAR T cell monotherapy. Our findings implicate that strategies to inhibit PD1 signaling in ICAM1-CAR T therapy has a potential to control advanced thyroid cancers and reduce off-tumor toxicities of CAR T cells *in vivo*.

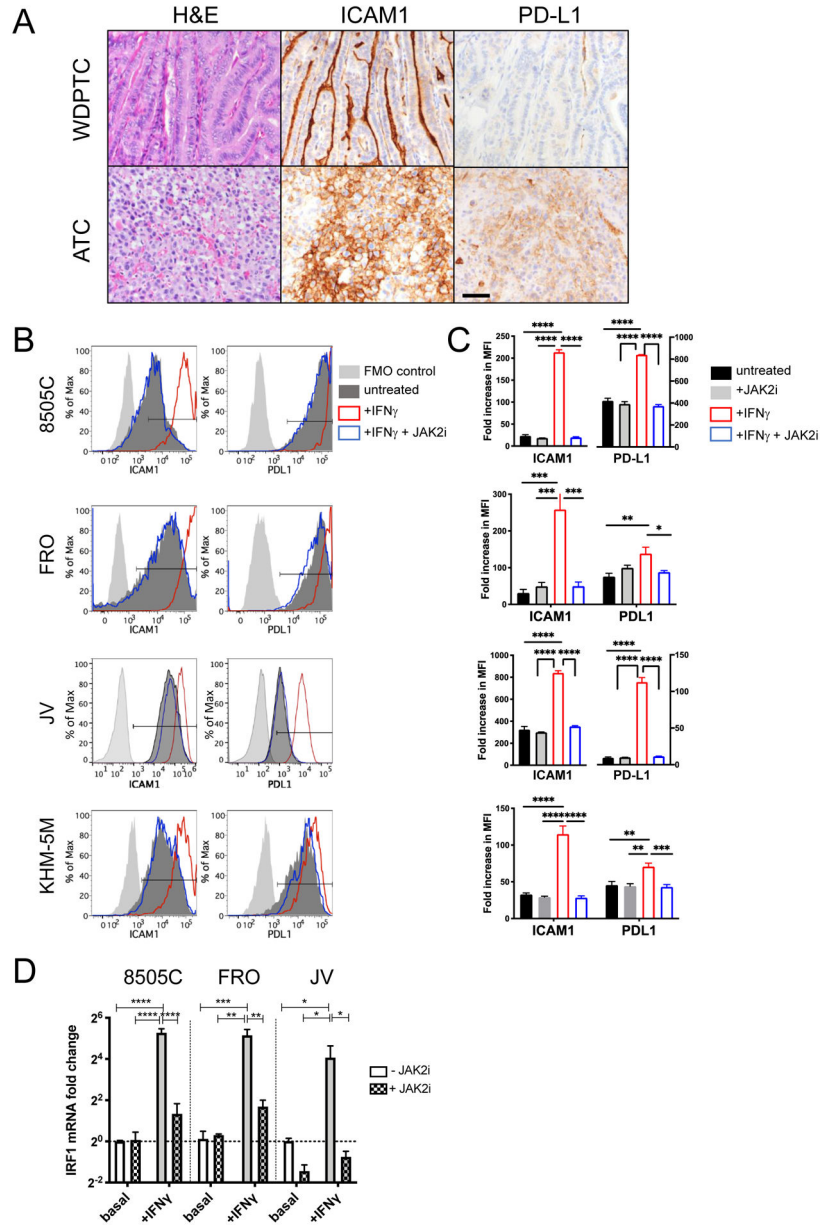


Figure 1. Expression and induction of ICAM1 and PD-L1 in thyroid tumor tissues and cell lines. (A) Representative images showing H&E staining, ICAM1 IHC, and PD-L1 IHC of tumor tissues from WDPTC and ATC patients. Scale bar = 20 μ m. (B) The surface expression of ICAM1 and PD-L1 was measured by flow cytometry. IFN γ (200 U/ml) with or without JAK2 inhibitor AZD1480 (1 μ M) were added for 48 hours to examine its effect on ICAM1 and PD-L1 expression. The gates for positively stained cells are marked with horizontal bars within the plots. (C) The fold increases in mean fluorescence intensity (MFI) of ICAM1 and PD-L1 were normalized to fluorescence minus one (FMO)-stained control cells. Data represents mean \pm sem. $n = 4 - 10$ replicates. The analysis was repeated independently at least three times. (D) qPCR measurement of *IRF1* mRNA expression in ATC cells 24 hours after IFN γ and/or AZD1480 treatment. Data represents mean \pm sem of three replicates. The

analysis was independently repeated at least two times. (*, $P < 0.01$; **, $P < 0.01$; ***, $P < 0.001$ by one-way ANOVA test (results were confirmed by the Kruskal-Wallis test)).

Author Manuscript

Author Manuscript

Author Manuscript

Author Manuscript

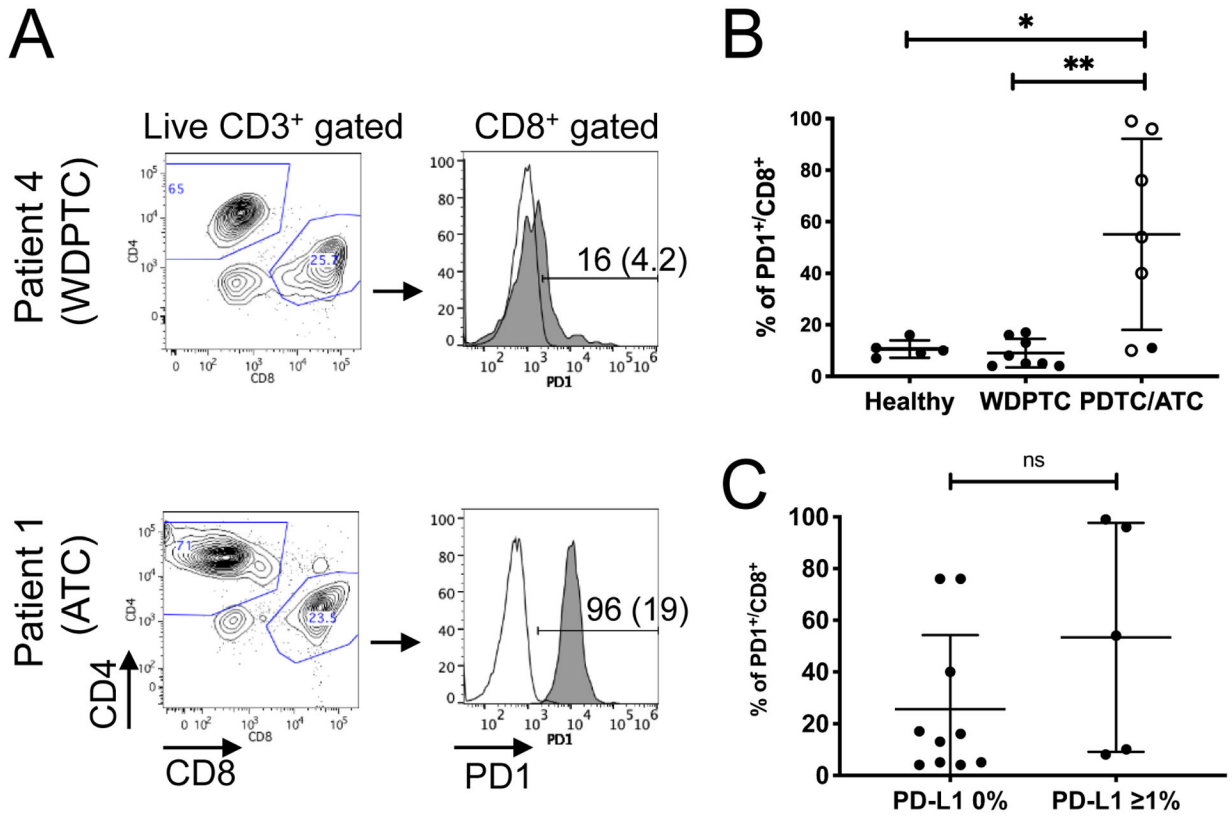


Figure 2. PD1 expression on T cells of thyroid cancer patients and healthy donors.

(A) Representative flow cytometry plots show CD4:CD8 distribution and PD1 expression from CD8⁺ T cells isolated from peripheral blood of thyroid cancer patients. The histogram plots show level of expression of PD1 (gray solid line) relative to FMO control (unfilled line). Percent positive for PD1 and MFI in parenthesis are shown. (B) The percentages of PD1⁺/CD8⁺ T cells are significantly higher in blood from PDTC/ATC patients compared to WDPTC patients or healthy donors. Open circles represent data from patients who presented lung metastasis at the time of diagnosis or recurrence (*, $P < 0.05$; **, $P < 0.01$ by Wilcoxon rank-sum test). (C) No significant correlation was observed in the percentages of CD8⁺/PD1⁺ T cells in thyroid cancer patient’s peripheral blood and PD-L1 expression in the tumor. ns = not significant. Statistical difference was analyzed using Wilcoxon rank-sum test.

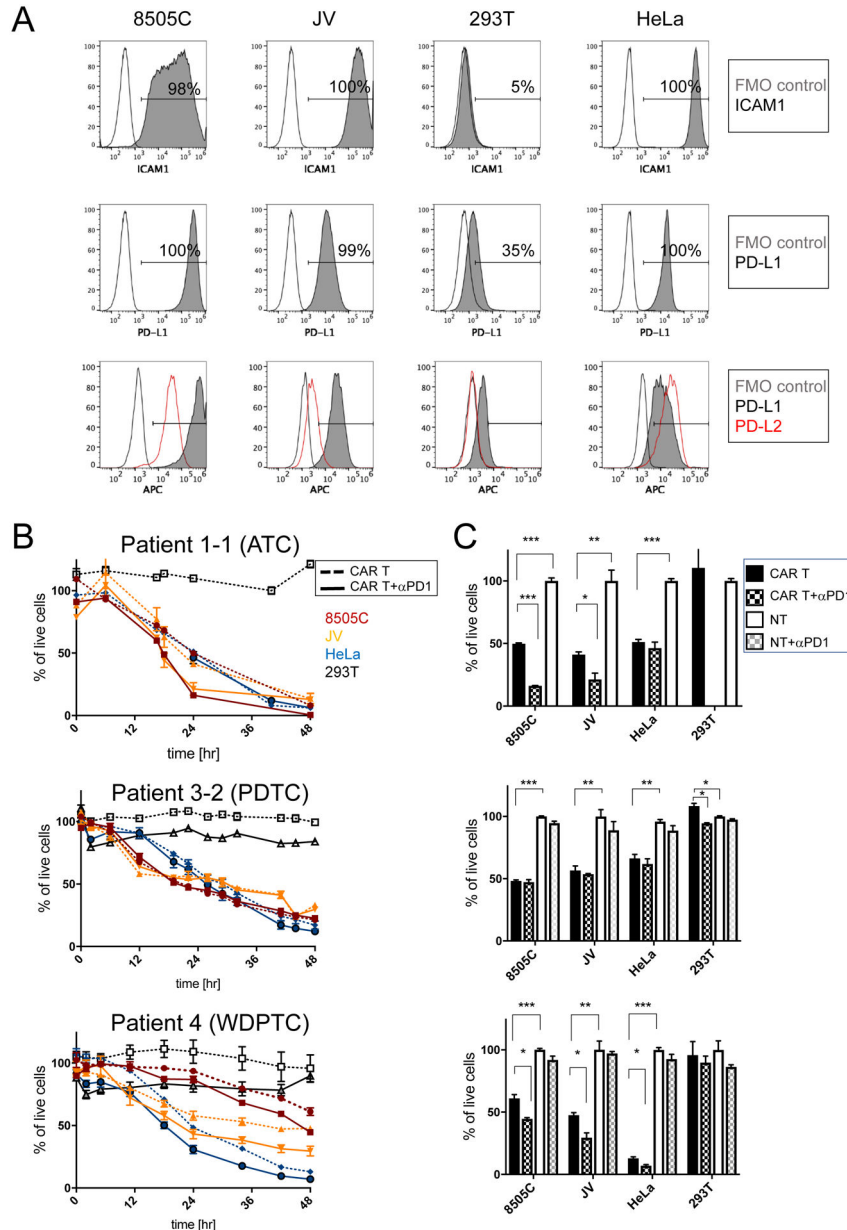


Figure 3. Inhibition of PD1 leads to increased target cell killing by ICAM1-CAR T cells *in vitro* independent of PD1 expression levels.

(A) Representative flow cytometry plots of ATC cell lines 8505C and JV, and 293T and HeLa control cell lines, which are stained for ICAM1 (first row) and PD-L1 (second row) antibodies. FMO control and antibody-stained plots are indicated by unfilled and gray solid lines, respectively. Flow cytometry plots showing the level of expression of PD-L1 (gray solid line) and PD-L2 (red line) relative to FMO control (unfilled line) (third row). (B) Cytotoxicity of thyroid cancer patient-derived ICAM1-CAR T cells (for donor and CAR T information, refer to Supplementary Table 1) against target ATC cell lines and control cells were examined in combination with PD1 blocking antibody. Peripheral T cells were isolated from patients with ATC, PDTC, and WDPTC. 5×10^3 target cells were co-cultured either with non-transduced T (NT) cells or anti-ICAM1 CAR T cells at a 2.5:1 ratio (1.25×10^4

cells) in media ($n = 3-7$ per group and representative of two to three independent experiments). (C) Differences in target cell killing were compared at a timepoint when approximately 50% of the 8505C cells were killed (24 hr for ATC, 22 hr for PDTC, and 48 hr for WDPTC). Statistical significance was determined by one-way ANOVA for CAR T vs. CAR T + α PD1 and CAR T vs. non-transduced T (NT) cells. *, $P < 0.05$; **, $P < 0.01$; ***, $P < 0.001$. Data represents mean \pm sem (results were confirmed by the Kruskal-Wallis test).

Author Manuscript

Author Manuscript

Author Manuscript

Author Manuscript

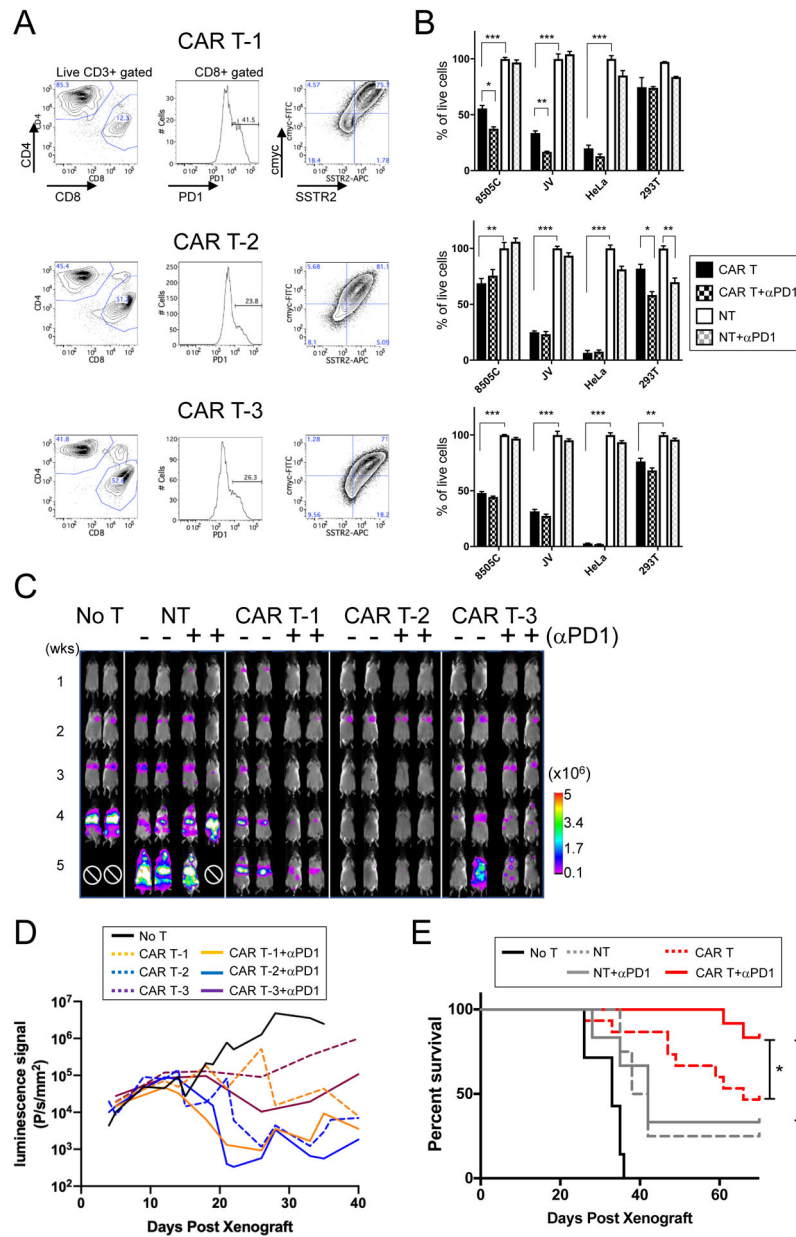


Figure 4. PD1 inhibition enhances the therapeutic efficacy and survival benefit of CAR T treatment in 8505C xenografts. (A) ICAM1-targeting mAS CAR T cells were generated from three commercial donor T cells using automated process via CliniMACS Prodigy (31). Flow cytometry plots are shown for the CD4:CD8 distribution among resting peripheral CD3⁺ T cells, PD1 expression in CD8⁺ T cells, and frequencies of *cmv*⁺ to estimate the CAR T lentiviral transduction rate and SSTR2⁺. (B) E:T assays were carried out with each donor CAR T and NT cells alone or with combination of anti-PD1 antibody (5 μg/ml). For each CAR T donor cells, matching NT cells from the same donor was used in the experiment ($n = 3$; *, $P < 0.05$; **, $P < 0.01$; ***, $P < 0.001$ by one-way ANOVA test; results were confirmed by the Kruskal-Wallis test). The analysis was independently repeated at least two times. (C) Representative weekly whole-body luminescence images of animals with 8505C xenografts, which received 10^6

ICAM1-CAR T (mAS) cells either with anti-PD1 antibody administration (+) or alone (-). Administration of CAR T (i.v.) and α PD1 antibody (i.p.) started ~5 days after 8505C injection into NSG mice. CAR T was a single treatment, while α PD1 antibody (150 μ g/mouse) administration was twice a week for 8 weeks. CAR T cells made from three different donor sources are shown. \emptyset marks the death due to tumor burden. (D) Quantitation of lung luminescence signals (P/s/mm²) over time in mice with 8505C xenografts treated with CAR T and α PD1, CAR T, or no treatment ($n = 7$ for no T; $n = 20$ for CAR T; $n = 12$ for CAR + α PD1 from donor-matched T cells; $P < 0.01$ for CAR T-1 vs. CAR T-1 + α -PD1 by Wilcoxon rank-sum test). (E) Survival curve of animals with 8505C xenografts with various treatments and no treatment is shown ($n = 7$ for no T; $n = 8$ for NT; $n = 6$ for NT + α -PD1; $n = 15$ for CAR T; $n = 12$ for CAR T + α -PD1; *, $P < 0.05$ by the log-rank test). For survival analysis, CAR T cells and matching NT cells from three different donors was combined.

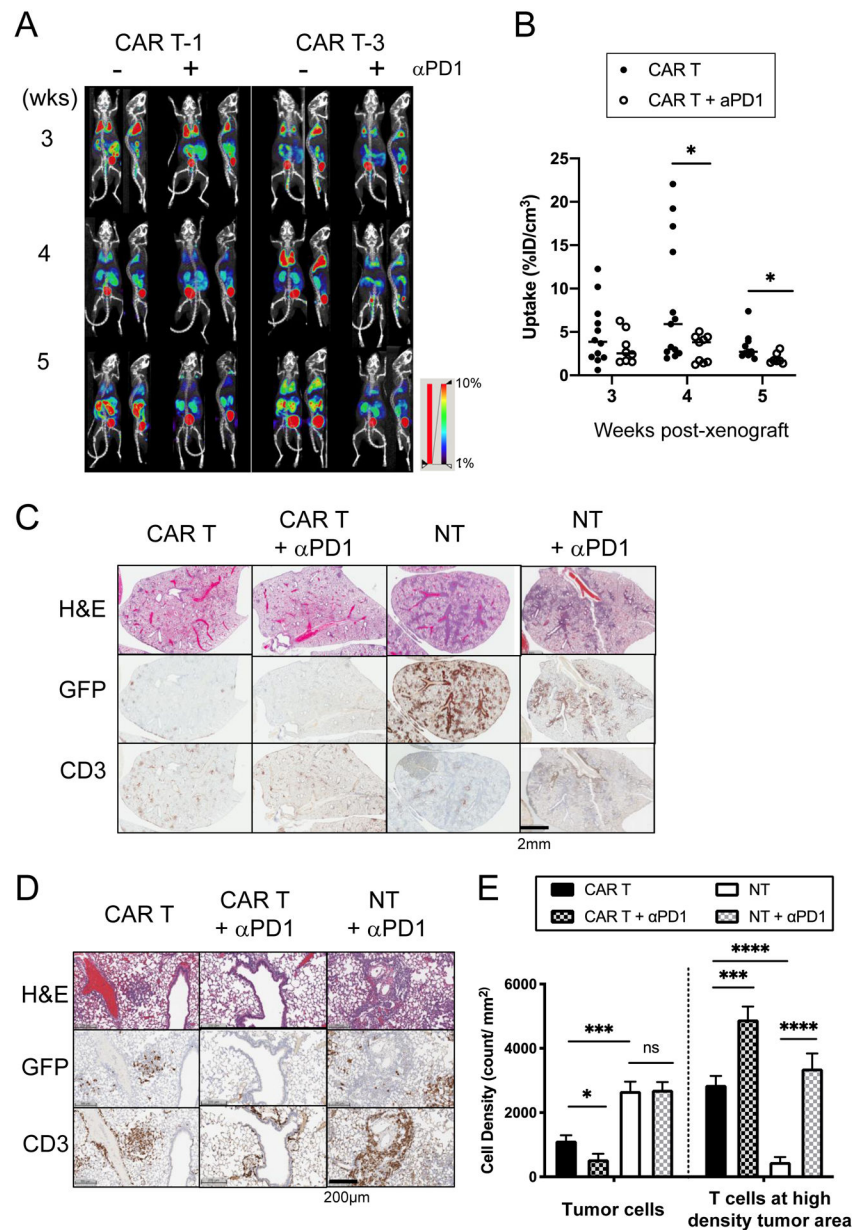


Figure 5. Administration of anti-PD1 antibody together with CAR T cells facilitated tumor killing and expansion of T cells specific to interaction with tumor cells *in vivo*.

(A) Longitudinal PET/CT images of NOTAOCT uptake in CAR T cells were taken in mice with 8505C xenografts treated with CAR T alone or co-administration of CAR T and anti-PD1 antibody. Images are maximum intensity projections of the entire mouse body (~20 mm-thick plane). PET intensity is pseudocolored in the range of 1–10%ID/cm³. (B) NOTAOCT uptake in the lung (%ID/cm³) were compared between CAR T and combination treatments of CAR T and anti-PD1 at each timepoint ($n = 11-13$ for CAR T; $n = 7-9$ for CAR T + α-PD1; *, $P < 0.05$ by Student's t-test. The same statistical significance was retained by Wilcoxon rank-sum test; scatter dot represents each animal and horizontal bar marks the mean in each treatment group). (C) Representative IHC images of H&E, GFP for tumor, and CD3 for T cell staining in the lung lobes of xenografts, which received different

treatments. (D-E) Quantitation of colocalization of CD3⁺ T cells and GFP⁺ tumor cells. Mouse lung tissues were harvested at 21 days post xenograft. (E) Cell density (absolute count/tissue area in mm²) was computed by digital analysis of CD3⁺ and GFP⁺ cells in high density tumor areas in the mouse lung. Two clusters of six different lung lobes from two mice were counted per treatment group ($n = 12$, *, $P < 0.05$; **, $P < 0.01$; ***, $P < 0.001$; ****, $P < 0.0001$ by Student's t-test).

Author Manuscript

Author Manuscript

Author Manuscript

Author Manuscript

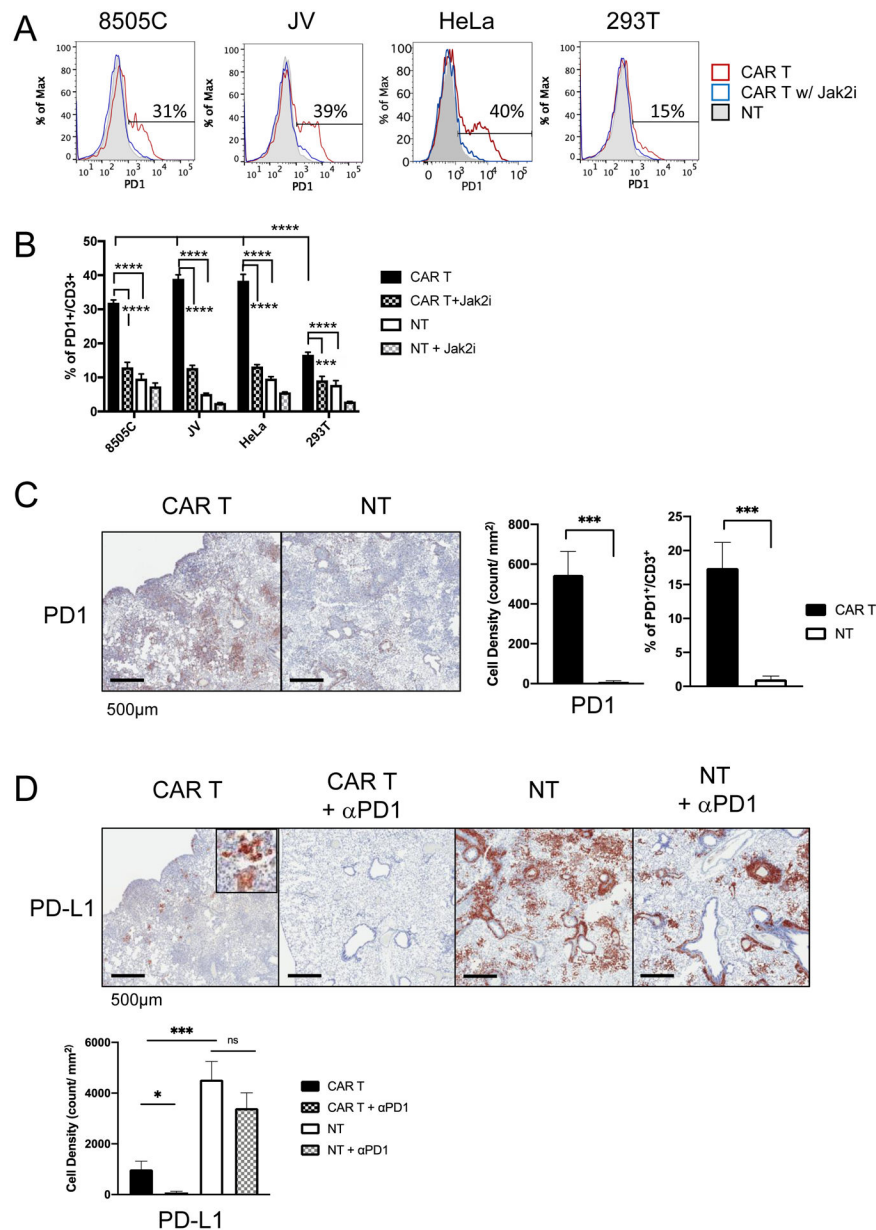


Figure 6. CAR T cell activity against tumor induces PD1 and PD-L1, which is rescued by anti-PD1 antibody in dual treatment.

(A) Representative flow cytometry plots of PD1 expression in T cells after incubation with target cells. ICAM1-CAR T (red line), NT (gray solid), and ICAM1-CAR T cells with JAK2 inhibitor AZD1480 (1 μ M) (blue line). (B) Quantitation of the frequencies of PD1⁺ cells among CD3⁺ T cells in co-culture of CAR T or NT with different target cells. Data represents mean \pm sem ($n = 4-7$; ***, $P < 0.001$; ****, $P < 0.0001$ by one-way ANOVA). (C) IHC images of PD1 in T cells infiltrating 8505C tumors in lung after CAR T or NT treatment. The cell density of PD1⁺ and CD3⁺ cells in the high density tumor spots in the mouse lung ($n = 8-9$ per group, data are combined from 1-2 tumor clusters in 3 distinct lung lobes from two mice for each group) was analyzed by an imaging analysis software (HALO). The percentages of PD1⁺ cells among CD3⁺ T cells were compared for lung sections after

CAR T or NT treatment (***, $P < 0.001$ by Student's t-test). (D) IHC images of PD-L1 staining in mouse lung xenografted with 8505C tumor after treatments with CAR T or NT with or without anti-PD1 antibody. The cell density of PD-L1⁺ cells in the high density tumor area in the mouse lung was analyzed ($n = 8-9$ per group; *, $P < 0.05$; ***, $P < 0.001$ by Student's t-test). Results confirmed by Wilcoxon rank-sum test and Kruskal-Wallis test, where applicable.

Author Manuscript

Author Manuscript

Author Manuscript

Author Manuscript

Table 1.

Clinicopathologic characteristics of thyroid cancer tissues included in the study.

	PD-L1 0% (n=20)	PD-L1 1% (n=13)	<i>P</i> value ^I
Histology			0.001
WDPTC	16 (84%)	3 (16%)	
PDTC	2 (100%)	0 (0%)	
ATC	2 (17%)	10 (83%)	
ICAM1 Expression			1.00
>1%	20 (100%)	13 (100%)	
ICAM1 Pattern			0.001
Apical	18 (86%)	3 (14%)	
Circumferential	2 (17%)	10 (83%)	
Clinical Characteristics			
Age	46 (37 – 62)	64 (38 – 83)	0.10
Male Sex	5/20 (25%)	2/13 (15%)	0.68
Tumor Size	1.8 (1.2 – 4.2)	3.5 (1.8 – 4.7)	0.19
Lymph Node Metastases	14/18 (78%)	4/7 (57%)	0.36
Distant Metastases	3/20 (15%)	7/13 (54%)	0.03
Lymphovascular Invasion	9/19 (47%)	8/11 (73%)	0.26
Gross Extrathyroidal Extension	3/20 (15%)	8/12 (67%)	0.01
BRAF ^{V600E} Mutation	14/17 (82%)	6/8 (75%)	1.00

^IP values were determined by Fisher's exact test